Front. Earth Sci. 2021, 15(2): 457–470
https://doi.org/10.1007/s11707-021-0878-9

RESEARCH ARTICLE

A quantitative study of the scale and distribution of tight gas reservoirs in the Sulige gas field, Ordos Basin, northwest China

Chao LUO (✉)[1,2], Ailin JIA[3], Jianlin GUO (✉)[3], Qing TIAN[4], Junlei WANG[3], Hun LIN[1], Nanxin YIN[1], Xuanbo GAO[1]

1 Chongqing University of Science and Technology, Chongqing 401331, China
2 Engineering Research Center of Development and Management for Low to Ultra-Low Permeability Oil and Gas Reservoirs in West China (Ministry of Education), Xi'an Shiyou University, Xi'an 710065, China
3 Research Institute of Petroleum Exploration and Development, PetroChina, Beijing 100083, China
4 Zhejiang Ocean University, Zhoushan 316022, China

Abstract Gas and water distribution is discontinuous in tight gas reservoirs, and a quantitative understanding of the factors controlling the scale and distribution of effective reservoirs is important for natural gas exploration. We used geological and geophysical explanation results, dynamic and static well test data, interference well test and static pressure test to calculate the distribution and characteristics of tight gas reservoirs in the H_8 Member of the Shihezi Formation, Sulige gas field, Ordos Basin, northwest China. Our evaluation system examines the scale, physical properties, gas-bearing properties, and other reservoir features, and results in classification of effective reservoirs into types I, II, and III that differ greatly in size, porosity, permeability, and saturation. The average thickness, length, and width of type I effective reservoirs are 2.89, 808, and 598 m, respectively, and the porosity is $> 10.0\%$, permeability is $> 10 \times 10^{-3}$ μm^2, and average gas saturation is $> 60\%$. Compared with conventional gas reservoirs, tight gas effective reservoirs are small-scale and have low gas saturation. Our results show that the scale of the sedimentary system controls the size of the dominant microfacies in which tight gas effective reservoirs form. The presence of different types of interbeds hinders the connectivity of effective sand body reservoirs. The gas source conditions and pore characteristics of the reservoirs control sand body gas filling and reservoir formation. The physical properties and structural nature of the reservoirs control gas–water separation and the gas contents of effective reservoirs. The results are beneficial for the understanding of gas reservoir distribution in the whole Ordos Basin and other similar basins worldwide.

Keywords tight gas, sandbody scale, effective sand reservoir, Ordos Basin

1 Introduction

The increasing use of natural gas has led to the rapid development of unconventional gas exploration and exploitation (Economides and Wood, 2009; Nelson, 2009; Liu et al., 2015a; Ju et al., 2018). The focus of gas field development has shifted from medium–high-quality reservoirs to low-quality reservoirs (Daniel and Viktor, 2015; Guo et al., 2015; Zafar et al., 2020). As such, tight sandstone gas reservoirs have increasingly become the focus of research (Ziarani et al., 2012; Behmanesh et al., 2014; Abuamarah et al., 2019). China contains rich tight gas resources. A number of large-scale, tight sandstone gas fields have been developed in the Upper Paleozoic in the Ordos Basin and Triassic Xujiahe Formation in the Sichuan Basin, which have become important sites of natural gas production (Hu et al., 2018; Li et al., 2019a, 2019b; Zou et al., 2019). In tight sandstone reservoirs with poor physical properties (Morad et al., 2010; Abdulrauf et al., 2019; Li et al., 2020a), there are still reservoirs with relatively good physical properties that are economically viable with existing development technologies (Davy et al., 2007; Yuan et al., 2014; Fu et al., 2015). Such reservoirs are termed "effective reservoirs" (Luo et al., 2016a). For example, in the Sulige gas field of the Ordos

Received August 4, 2020; accepted February 1, 2021

E-mails: lc_121989@163.com (Chao LUO),
guojianl@petrochina.com.cn (Jianlin GUO)

Basin, field logging and gas production has shown that effective reservoirs in the H_8 Member have lower physical property limits of 5% for porosity, 0.1×10^{-3} μm^2 for permeability, 50% for gas saturation, and < 70 API for the gamma logging value.

The scale of an effective reservoir determines the geological reserves of a single well (Luo et al., 2016b). However, due to the discontinuous distribution of gas and water in tight gas reservoirs and differences in effective reservoir scales, it is difficult to calculate the geological reserves of tight gas reservoirs (Jia et al., 2018). It is often found that the estimated reserves in the initial stages of development are larger than those found in the actual development process (Ostensen, 1983; Shanley et al., 2004; Morteza et al., 2015). The differences between the proven and calculated reserves are mainly due to: 1) the single sand bodies that were thought to be distributed continuously between wells actually being distinct (Tye, 2004; Wang et al., 2018), with thinning and pinching between wells resulting in a lower gas-bearing reservoir volume; 2) multiple wells showing that the scale of the channel sand bodies and effective reservoirs is small, the interpolation and extrapolation of the gas-bearing sand bodies was too optimistic, and the gas-bearing area was initially overestimated (Liu et al., 2014); 3) strong lateral variations in reservoir quality resulting in a reduction of the gas-bearing reservoir volume; and 4) the full range of reservoir evaluation parameters not being properly considered, and only including parameters such as porosity, permeability, gas saturation, median particle size, and pore throat radius (Zou et al., 2012; Wang et al., 2017), and not taking into account the most important parameter i.e., reservoir size.

Based on previous studies (Amiri et al., 2012; Jiang et al., 2020; Li et al., 2020b), the conventional evaluation method has many disadvantages for tight gas reservoirs with strong heterogeneity (Zhao et al., 2009; Miller and Shanley, 2010). Here we propose a new method for quantitatively evaluating the scale of tight gas reservoirs. Various macro- and micro-scale parameters of different types are used to analyze the factors controlling the scale of effective tight gas reservoirs, which can improve the accuracy of reserve estimations. Natural gas reserves are the material basis of gas field development. Reserve calculation and evaluation is a long-term project throughout the exploration and development stages of gas reservoirs (Chen et al., 2015; Liu et al., 2015b). With increasing data, it is necessary to constantly recalculate and re-evaluate natural gas reserves. The gas-bearing area and effective thickness are important parameters that affect the calculation of reserves. Analysis of effective reservoir size and distribution of tight gas provides accurate calculations of reserves in tight gas reservoirs. This method is also significant for optimizing single-well productivity evaluation, formulating development technology, and improving exploitation of tight gas reservoirs. Effective reservoirs of tight sandstone are generally those with relatively good physical properties, but with low porosity and permeability (Santamarina et al., 2019; Wang et al., 2020). Many studies have proposed evaluation parameter systems for effective tight gas reservoirs. However, the effective reservoir size is often neglected, but is of significance in well pattern deployment. Accurate determination of the effective reservoir scale guides the optimization of well spacing, which can maximize the reserves and exploitation. If the well spacing is too large, some effective reservoirs between wells will not be drilled, resulting in a lower recovery rate. If the well spacing is too small, it will increase the probability of two wells drilling the same sand body at the same time, increase inter-well interference, and lead to a reduction in the cumulative gas production of a single well. The optimization of the well pattern requires knowledge of the reservoir geology, gas reservoir engineering, and production dynamics.

2 Geological setting

The Sulige gas field is located in the Ordos Basin, and is currently the largest tight sandstone gas field in China (Fig. 1). Its proven reserves are 4.7×10^{12} m^3 and the reserve abundance is ~1.5×10^8 m^3/km^2. The reserve abundance is generally low and has a planar differential distribution. In the past five years, production of the Sulige gas field has exceeded 220×10^8 m^3/a (Zhao et al., 2013). The Su 6 and Su 36 areas are typical blocks in the Sulige gas field.

The Sulige gas field reservoir is generally tight and has a large thickness of sandstone. The effective reservoirs are coarse-grained sandstone lenses, surrounded by thickly bedded sandstones with poor physical properties. Experimental analysis has shown that the overburden permeability of > 85% of the samples is $< 0.1 \times 10^{-3}$ μm^2. During sedimentation of the host rock formation, thick, braided river sand bodies formed widely in the northern Ordos Basin. Coal-bearing source rocks led to the sedimentary sand bodies becoming gas-bearing, with the degree of gas enrichment being positively correlated with the physical properties of the sand bodies. Effective reservoirs were developed in the coarse-grained sandstone with better physical properties (i.e., braided river bar and channel deposits), and their gas saturation is higher than that of the surrounding sand bodies (He et al., 2013). The effective reservoirs are small in scale and have poor lateral connectivity. Effective reservoirs comprising multiple non-connected layers overlap and are widely distributed. Two to four effective reservoirs can be drilled in a single well. These effective reservoirs can be distributed over tens of thousands of square kilometers.

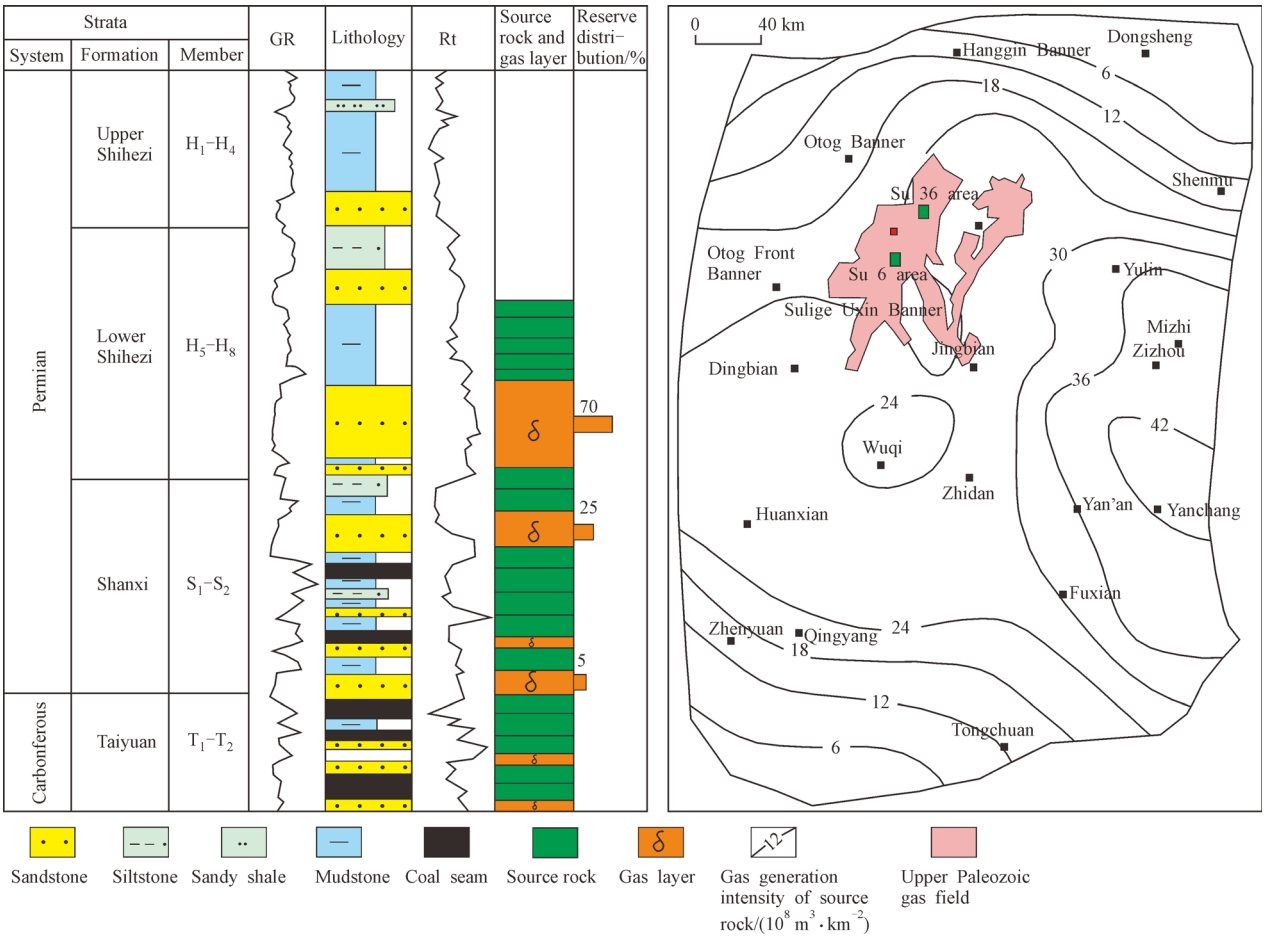

Fig. 1 Late Paleozoic stratigraphy and distribution of source rocks and the H_8 Member reservoir in the Ordos Basin (GR = Gamma Ray; Rt = Resistivity).

3 Methods

Numerous studies have investigated the scale of braided river reservoirs (John and Peter, 1997; Bersezio et al., 2007) using a variety of methods, including investigations of modern sedimentation (Hooke, 2003; Lunt et al., 2013), field geology (Labourdette, 2011), and well logs (Bridge and Tye, 2000). However, the scale of these studies is mainly at the level of a single sand body, which corresponds to the scale of an isolated composite sand body. Based on dynamic and static data, we quantified the scale of braided river effective reservoirs in the H8 Member of the Shihezi Formation in the Sulige gas field. This was achieved by integrating data from numerous wells and the results of interference and static pressure testing, which mainly yielded thickness and areal extent data for different types of effective reservoirs.

3.1 Sandstone distribution characterization

Multiple wells enable geological and geophysical data to be used to undertake reservoir correlations between wells. Reservoir connectivity at a certain well spacing and reservoir size can be examined by statistical analysis. The effective reservoir thickness can be determined from rock electrical properties (Smith et al., 2006), and effective reservoir size can be estimated from the width or length/thickness ratio of sedimentary bodies observed in the field (Martin, 2006; Guo et al., 2017).

3.2 Interference well testing

The interference well test is an important method of assessing the degree of reservoir connectivity between wells. This test uses a pair of wells, one of which is the "excitation well". Varying the operational conditions of the excitation well during well testing changes the formation pressure in the "observation well". During testing, the observation well is shut down and a downhole pressure gauge is used to record the changes in formation pressure. The reservoir connectivity between wells can be assessed by analyzing the pressure variations in the observation well(s).

3.3 Static pressure test

Some wells in the study area have been in production for several years. If the effective reservoirs in new wells are connected with those of adjacent older wells, the production of the older wells will reduce the formation pressure in the infilled wells (Ji et al., 2019). The average pressure coefficient of the H_8 Member is ~0.82. The depth of the formation can be used to infer the original formation pressure. For example, the original formation pressure of the H_8 Member in the Su 6 area is ~30 MPa, and the pressures of several infilled wells remain close to this value, which shows that the infilled wells are not connected with the adjacent older producing wells.

4 Results

4.1 Sandstone distribution characterization

The braided river sand bodies of the H_8 Member are up to tens of meters thick and laterally continuous over tens of square kilometers. The effective reservoir is the gas-bearing part of the sand body. Braided river bar and channel deposits form the effective reservoirs in the H_8 Member. Core calibration logging was used to identify the intervals of gas-bearing sand bodies. The main gas-bearing sand body comprises medium–coarse-grained sandstone with cross bedding and a massive, gravel-bearing, coarse-grained sandstone. The effective reservoirs are thin, dispersed, and have a uniform thickness (1.5–5.0 m; average = 2–3 m). The total effective reservoir thickness formed by vertical stacking of multiple individual sand bodies is 3–6 m. The average effective reservoir thickness in a well is positively correlated with the number of effective single sand bodies intersected by drilling. Field outcrops in Liulin and Hancheng, Shanxi Province, of the target strata in the Sulige gas field were described, analyzed, and compared. The thickness and lateral extent of the medium–coarse-grained and massive gravel-bearing coarse-grained sandstone facies in bar and channel deposits were determined. Due to the various interbeds developed in a braided river sedimentary system, the scale of a single effective gas-bearing sand body is small (up to 300 m), and the lateral extent of effective reservoirs in some areas is < 100 m. According to these field observations, the sand bodies have a width/thickness ratio of 40–80 and, as such, the effective reservoir extent in the Sulige gas field is 60–400 m and the effective reservoir length is 90–1200 m, given the 1.5–3.0 length:width ratio of the braided river sand bodies.

Due to the increasing number of gas wells in the Sulige gas field, the well spacing has reduced from 1600 to 800 m, or even 400 m. This has led to the estimated scale of single sand bodies becoming smaller, which means the effective reservoir is highly heterogeneous, poorly connected, and smaller scale than originally thought.

For example, for wells S6 and S38-16-4, the original well spacing was 1621 m, but wells S38-16-3, S6-J4, and S6-J14 have been subsequently drilled. Four gas-bearing sand bodies are present in the S6 well, and three gas-bearing sand bodies are present in the S38-16-4 well. The width of the sand body is apparently > 1500 m. Subsequent data from the new wells confirmed that the effective reservoir size is small, with a lateral extent of < 400 m. The No. 2 sand body in well S6 is connected with the No. 2 sand body in well S38-16-3, and the corresponding gas-bearing sand body at this depth is missing in well S6-J4, which indicates that the No. 2 sand body in well S6 is not connected with the No. 2 sand body in well S38-16-3. Thus, the lateral extent of this effective reservoir is < 800 m (Fig. 2).

4.2 Interference well testing

Many interference well tests have been undertaken to calculate the size of effective reservoirs in the Sulige gas field. In 2013, an interference test of five well groups was carried out in the S36-11 area using S36-2-21 as the excitation well (Fig. 3). Two well groups experienced interference, indicating that S36-2-21 is connected with the S36-J2 and S36-J6 wells. Well S36-2-21 was placed into operation on December 17, 2007. The daily gas production was $\sim 1.96 \times 10^4$ m^3/d, casing pressure was 13.4 MPa, and cumulative gas production was 4382.3×10^4 m^3 during the interference test. The S36-J1 and S36-2-21 well intervals were not connected, as the pressure rose during the test. The connected S36-J2 and S36-2-21 sand bodies are in the lower part of H_{8x}^2 (Fig. 4), and the effective reservoir width is > 560 m (i.e., the well spacing). Well S36-2-21 only intersected H_{8x}^1, which is not the same sand body as in wells S36-J4 and S36-J5 (i.e., H_{8x}^2). It can also be determined from the pressure recovery time that wells S36-J2 and S36-J6 are connected to well S36-2-21. Compared with the other wells, the pressure recovery times of S36-J2 and S36-J6 were only 65.03 and 64.96 d, which is much shorter than the other wells (Table 1). In wells S36-J4 and S36-2-21, there is a facies change at the top of H_{8x}^2, and the effective reservoir continuity is poor. Wells S36-J5 and S36-2-21 intersected the top of H_{8x}^2, which is not the same single layer (Fig. 4), and the effective reservoir connectivity is poor and less than the well spacing (737 m).

4.3 Static pressure tests

Numerous static pressure tests have been undertaken to calculate the size of effective reservoirs in the Sulige gas field. In 2013, eight infilled wells (S36-J1 to S36-J8) were subjected to a static pressure test. The test results showed that the pressure of the S36-J7 well (29.41 MPa) is normal

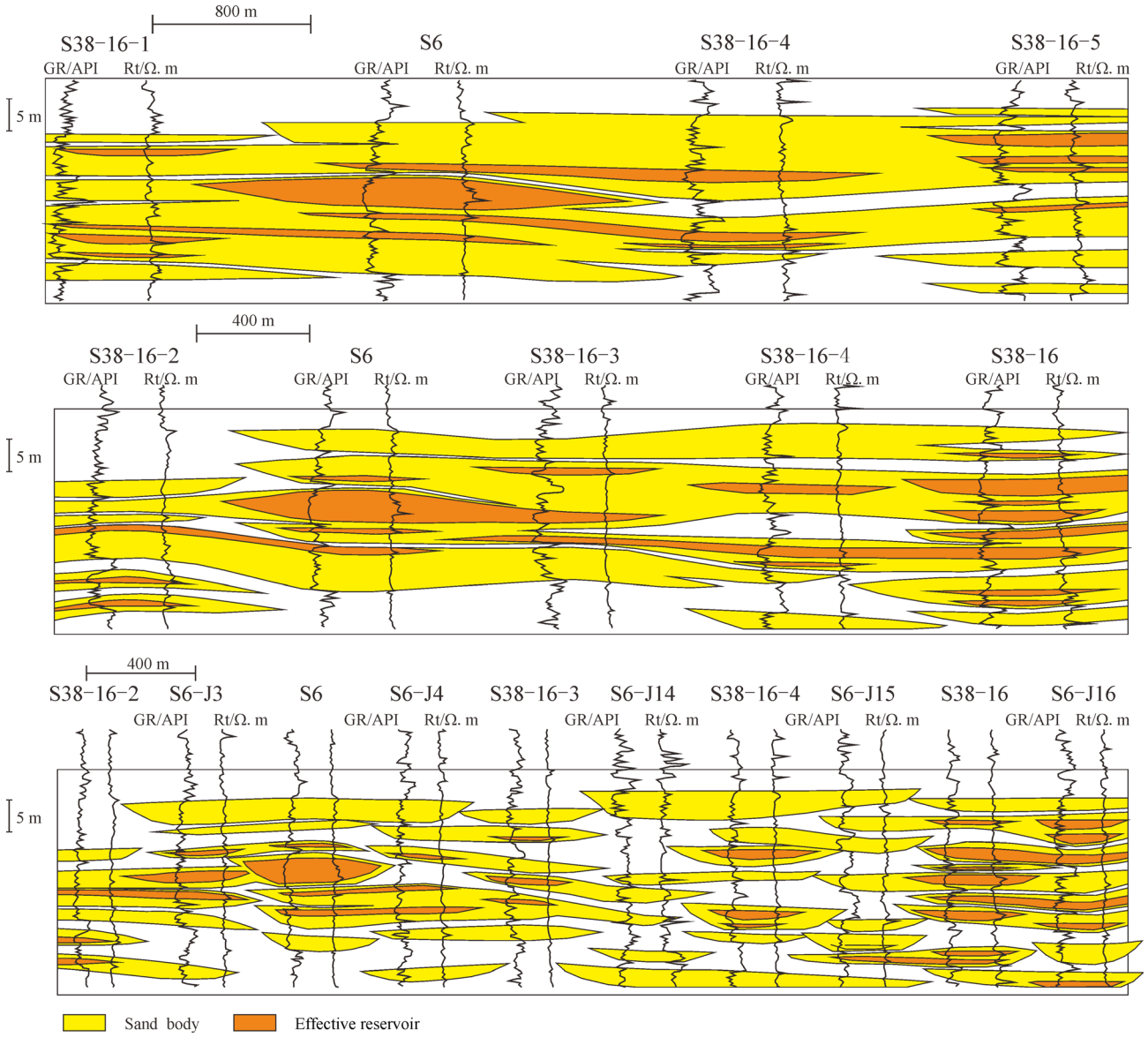

Fig. 2 Distribution of tight gas effective reservoirs in a densely drilled area of Su 6 (see Fig. 1 for location).

Table 1 Interference well test data for the S36-2-21 well block

Well name	Recovery test days	Pressure recovery/MPa			
		Day 1	Day 66	Day 67	Day 109
S36-J1	108.13	18.77	18.95	18.95	19.00
S36-J2	65.03	21.12	20.98	/	/
S36-J4	108.64	21.16	21.65	21.71	21.94
S36-J5	108.12	17.83	18.05	18.08	18.23
S36-J6	64.96	23.09	22.74	/	/

and, in the remaining seven wells, is significantly lower than the original formation pressure (29–31 MPa). This shows that the static pressure disturbance occurs over a (300–500) m × (300–400) m well grid, and thus the effective reservoir extent is > 500 m. The production of well S36-3-20 has had an obvious effect on well S36-J8, indicating that the effective reservoir is connected between these two wells, with an extent of > 431 m. Well S36-J7

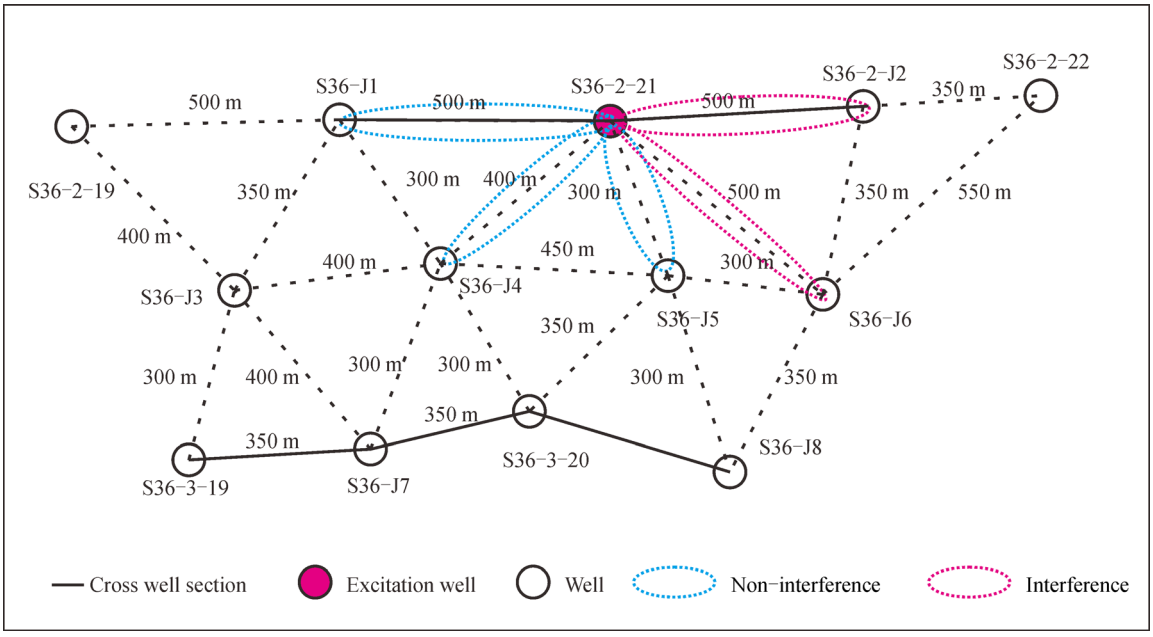

Fig. 3 Well location of interference tests conducted in well block Su 36 (see Fig. 1 for location).

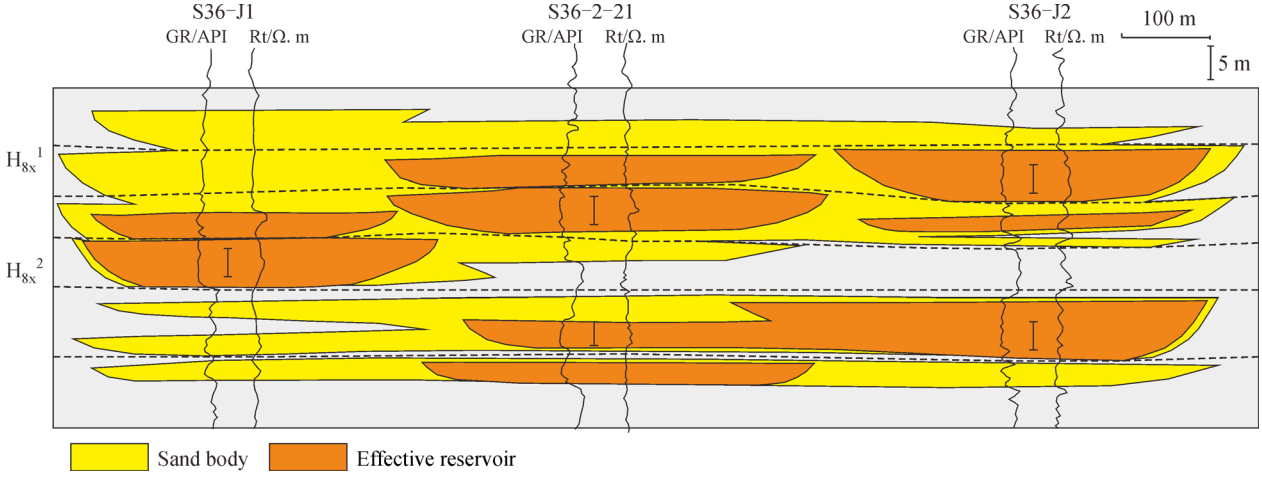

Fig. 4 Schematic cross-section of the results of the interference test.

(29.41 MPa) had no static pressure disturbance, and thus the effective reservoir extent towards well S36-3-20 is < 350 m (Fig. 5).

Field observations and interference and static pressure test data were used to analyze the lengths and widths of 100 effective reservoirs (Fig. 6). For instance, there are 13 wells in the S36-2-21 wellblock. According to the plane distribution diagram of various types of effective reservoirs in $H8_x^{1-3}$ layer of S36-2-21 wellblock, effective reservoirs are developed in all wells except well S36-2-22. Wells that develop type III effective reservoirs are S36-J2, S36-J5 and S36-3-J19. Wells that develop type I effective reservoirs are well S36-2-21, S36-3-20 and S36-J8. The rest 6 wells all develop type II effective reservoirs. It accounts for 46.15% of the total number of wells. Type II effective reservoirs are the most common type of reservoir. The effective reservoir size in the Sulige gas field is relatively smaller than a conventional gas reservoir. The length and width of effective reservoir type I is > 700 m and > 500 m, respectively. The length and width of effective reservoir type II are 400–700 m and 200–500 m, respectively, and for the type III effective reservoir are < 400 m and < 200 m (Fig. 7). Type II and III effective reservoirs account for > 70% of all the effective reservoir.

Statistical features of the type I, II, and III effective reservoirs were calculated, including the average thickness, length, width, porosity, permeability, and gas saturation. The average thickness, length, and width of effective reservoir type I are 2.89, 808, and 598 m, respectively, with porosity > 10.0%, permeability > 10×10^{-3} μm^2, and a gas saturation of ~60%. The average thickness, length, and width of effective reservoir type II

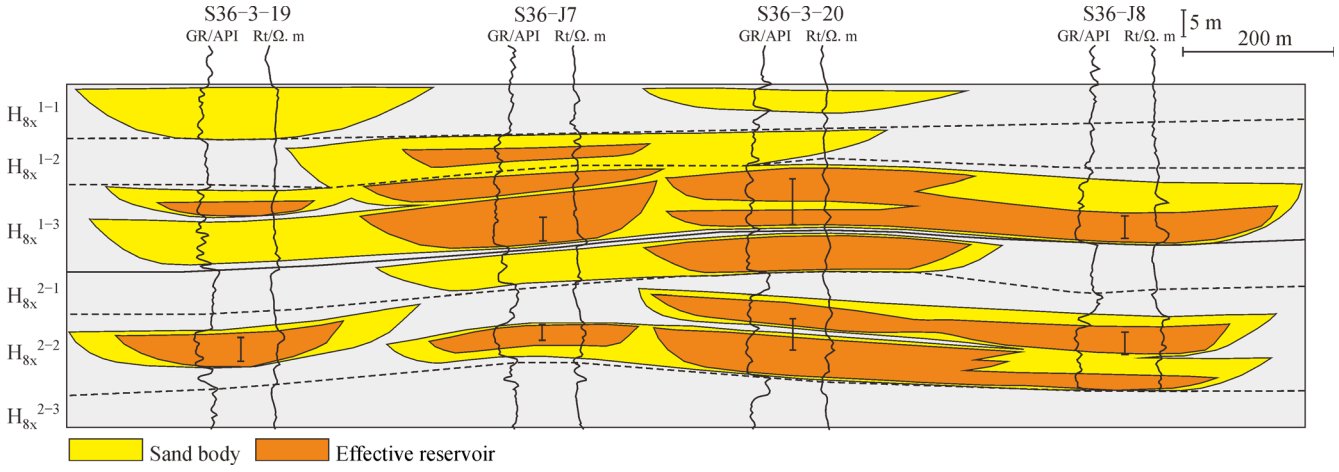

Fig. 5 Schematic cross-section showing the results of static pressure testing.

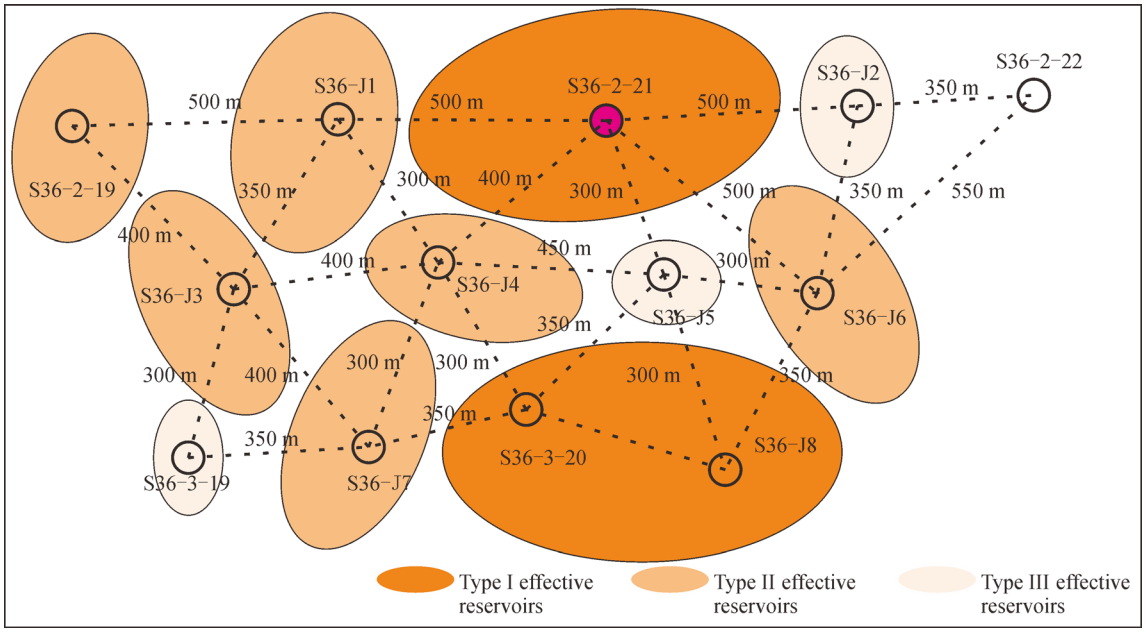

Fig. 6 Planar distribution of different types of effective reservoirs in the single layer H_{8x}^{1-3} of the S36-2-21 well block.

are 2.13, 537, and 386 m, respectively. The average porosity is 7.5%–10.0%, average permeability is 1.0×10^{-3}–10×10^{-3} μm², and average gas saturation is 55%–60%. The average thickness, length, and width of the type III effective reservoir are 1.58, 357, and 149 m, respectively. The average porosity is 5.0%–7.5%, average permeability is 0.1×10^{-3}–1.0×10^{-3} μm², and average gas saturation is 50%–55% (Table 2).

5 Discussion

5.1 Scale of the sedimentary system

Reservoir formation in the Sulige gas field was affected by strong compaction, cementation, dissolution, and diagenesis, which profoundly changed the reservoir (Fan et al., 2014). Due to sedimentary and diagenetic controls, the effective reservoirs are highly dispersed and comprise high-permeability units within a generally low-permeability lithology. The effective reservoirs are mainly isolated, although a few are vertically superimposed and locally horizontally connected. The effective reservoirs are coarse-grained sandstones from the middle and lower parts of river bar and channel deposits. Coarse-grained sandstone facies, such as those at the bottoms of channels and in bars, experienced strong hydrodynamic conditions, have good sorting, and are relatively pure in terms of lithology. Due to the high content of rigid grains, such as quartz, primary pores can be preserved during deep burial, which result in relatively good reservoir connectivity. The primary pores were enhanced by later dissolution, which

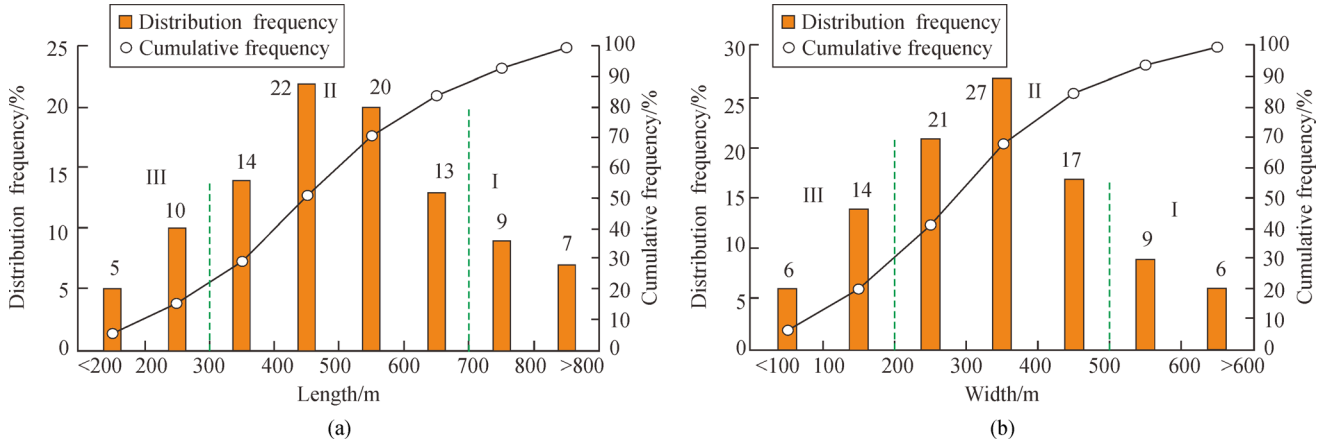

Fig. 7 Effective reservoir length and width in the Sulige gas field. (a) Distribution frequency of the effective reservoir length; (b) distribution frequency of the effective reservoir width.

Table 2 Properties of type I, II, and III effective reservoirs

Effective reservoir type	Average thickness/m	Average length/m	Average width/m	Porosity/%	Permeability ($\times10^{-3}$/um^{-2})	Gas saturation /%
I	2.89	808	598	> 10.0	> 10.0	> 60.0
II	2.13	537	386	7.5–10.0	1.0–10.0	55.0–60.0
III	1.58	357	149	5.0–7.5	0.1–1.0	50.0–55.0

provided a pathway for fluid migration. Therefore, the typical size of river channels and bars had a control on the scale of these effective reservoirs. According to Miall (2006), distributary channels and bars form composite sand bodies (i.e., a single channel belt). The scale of a single channel belt can provide a clearer understanding of the sizes of distributary channels and bars (Skelly et al., 2003).

A single channel belt can be investigated from field outcrops, well correlations, three-dimensional seismic data, and empirical formulae (Nazari et al., 2019). Although three-dimensional seismic data exist for the Sulige gas field, it is of limited resolution, and thus the well correlation and empirical formulae methods were used to determine the scale of the single channel belts in the target strata. The key factor in determining the horizontal distribution of the channel by well correlation is to determine the boundary of the channel belt. The main features that indicate the boundary of the channel belt are: 1) overbank mudstone deposits; 2) abandoned channel sediments; 3) differences in sedimentary cycles; and 4) elevation differences in the channel sand bodies. In well S13, the overlapping river facies are easily identified in a single well using the above features. When examining the channel sand body in the E–W direction, for which the well spacing is 300–500 m, the channel width is estimated at 662–1663 m and the paleocurrent directions are mainly N–S. Therefore, a single channel crosses 2–5 wells. Subsequently, the sand bodies of the connected channel belt can be identified in the adjacent wells. Therefore, the sand bodies of a given channel belt should have an approximate width in the N–S direction (Fig. 8).

Bridge (1993) presented formulae (Eqs. (1) and (2)) linking the minimum width (W_{cbmin}) and maximum width (W_{cbmax}) of a single braided belt to the average single channel full bank depth (h_a). These formulae were verified by studies of field outcrops. We used these empirical formulae to predict the width of a single braided belt. The average single channel full bank depth (h_a) was calculated from the single channel full bank depth (h_d) (Eq. (3)). The average depth of a single channel in the Sulige area is ~10 m. The estimated depth of a single channel is 3.3–7.7 m (average = 5.5 m). The calculated width of a single braided belt is 500–3100 m, and the average is ~1637 m. Therefore, it is difficult to form bars and channels with a scale of up to tens of kilometers in a braided belt system, which limits the scale of effective sand bodies that form during diagenesis.

$$W_{cbmin} = 59.9h_a^{1.8}, \quad (1)$$

$$W_{cbmax} = 192h_a^{1.37}, \quad (2)$$

$$h_a = 0.55h_d, \quad (3)$$

where h_a is average single channel full bank depth, m; h_d is single channel full bank depth, m; W_{cbmin} is minimum width, m; W_{cbmax} is maximum width, m.

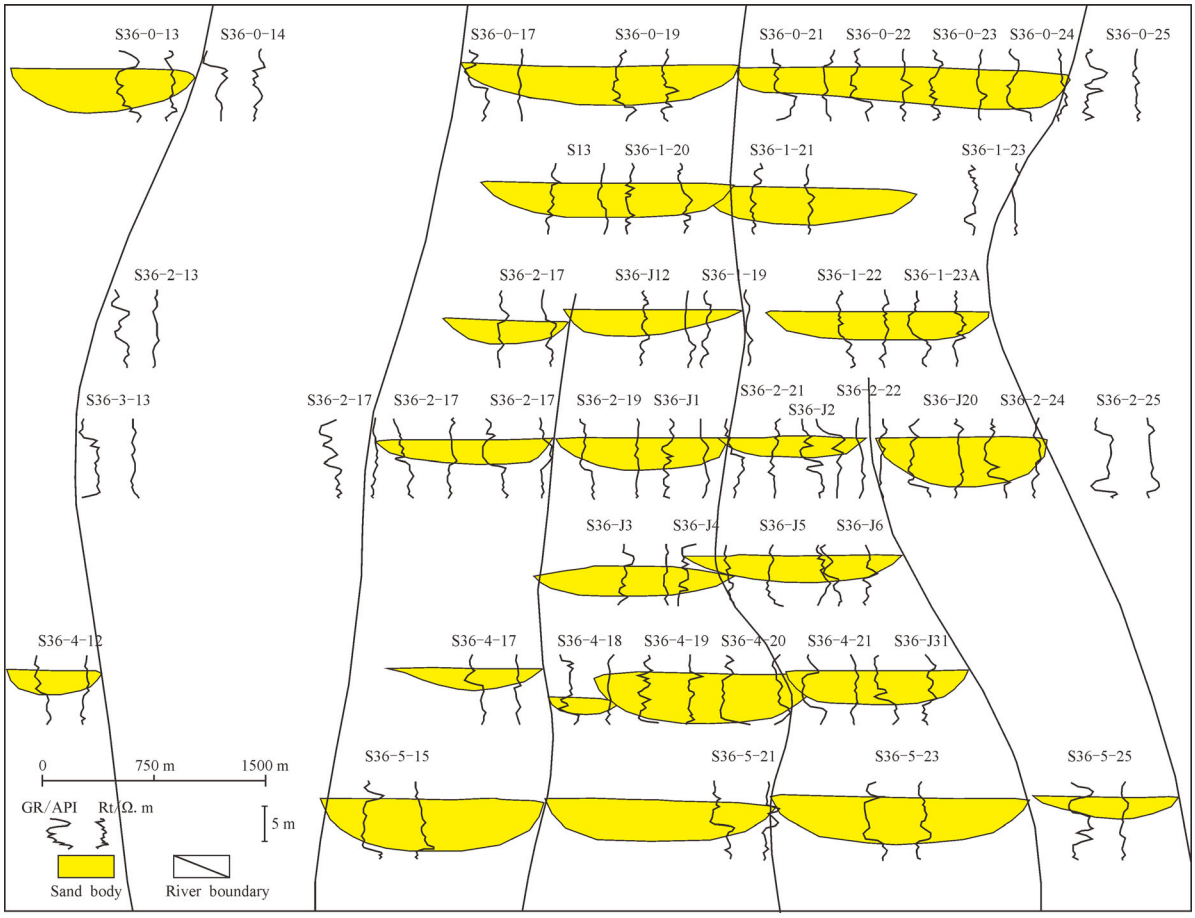

Fig. 8 Sedimentary system boundaries in the Sulige gas field.

5.2 Impacts of interbeds on the scale of tight gas reservoirs

The Sulige gas field contains a typical sandy braided facies reservoir of a tight gas field. Many horizontal wells have also been drilled in this area and have intersected various types of interbeds. The geometrical characteristics of each type of interbed are different and their relationships are complex. The presence of interbeds results in poor connectivity and a complex distribution of effective reservoirs. Field geology and modern sedimentary studies (Best et al., 2006) indicate numerous types of interbedded reservoirs are present in the H_8 Member, including overbank mud, interbar mud, silt layer, abandoned river channel, and gully deposits, which divide the effective reservoirs into smaller parts. A cross-section of connected wells from S36-3-19 to S36-J8 shows that interbeds are developed at different levels between sand bodies and inside single sand bodies in each well. The thickness range of effective single sand bodies in a single well is mainly 2–5 m, with a width/thickness ratio of 40–80. The effective reservoir width in most cases ($>80\%$) is <650 m and the length is <1000 m. The general lateral extent of the effective reservoirs is 300 m (Fig. 9).

5.3 Gas source conditions influence to reservoir saturation

Upper Paleozoic strata in the Sulige gas field are mainly Carboniferous and Permian coal-bearing and marine carbonate source rocks at the top of the Benxi, Taiyuan, and Shanxi formations (Li et al., 2020b). They all contributed to hydrocarbon generation. The hydrocarbon generation intensity in most areas is 12×10^8–28×10^8 m^3/km^2. Previous studies have shown that natural gas in the Sulige gas field mainly accumulated close to source, forming the main reservoir of the H_8 Member.

The gas source conditions affect the reservoir gas filling, which is related to the filling energy and pressure. The source–reservoir pressure variation of a simulation experiment on the Sulige tight gas reservoir showed that a tight reservoir, with a permeability of $<1.0 \times 10^{-3}$ μm^2, has an obvious intake pressure threshold, and the reservoir would only begin to inflate when the source–reservoir pressure difference reached a certain value. However, the source–reservoir pressure cannot be balanced immediately after intake, due to the tight, low permeability reservoir. With increasing gas pressure, the rate of reservoir gas infilling accelerates, and the pressure difference between the source

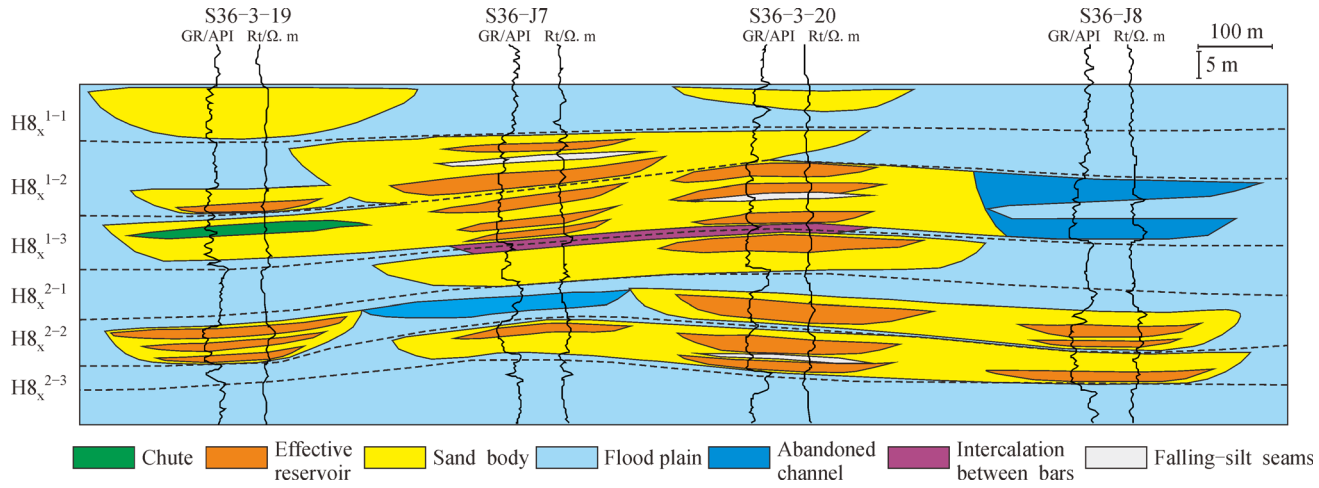

Fig. 9 Distribution of interbeds and effective sand bodies in the Su 36 area.

and reservoir decreases gradually until the balance pressure is reached. The lower the reservoir permeability, the higher the threshold pressure and source–reservoir balance pressure. As such, a tighter reservoir requires more rigorous filling conditions with higher filling energy and pressure (Xu et al., 2017). In contrast, gas saturation curves of rock samples with different permeabilities after filling at different pressures indicate that when the pressure reaches the threshold pressure, the gas saturation is low. With increasing gas source pressure, the gas saturation gradually increases, and the growth rate decreases over time. The poorest type of reservoir has low permeability (e.g., 0.029 $\times$ 10^{-3} μm^2) and cannot form an effective reservoir because the gas saturation does not exceed 30% after final filling. With better reservoir physical properties, the probability of gas saturation reaching the effective reservoir increases after filling. In general, gas saturation with a reservoir permeability of 10 $\times$ 10^{-3} μm^2 can be $>$ 60% (Fig. 10).

At the end of reservoir gas filling, the effective reservoir often shows macroscopic variations in gas–water distribution and gas production characteristics. Due to migration and accumulation, areas with high hydrocarbon generation intensity are mostly gas-enriched, and areas with low hydrocarbon generation intensity are mostly gas–water reservoirs. The Sulige gas field has a surrounding hydrocarbon generation intensity of 16 $\times$ 10^8 m^3/km^2, and has gas reservoirs in its central region and gas–water reservoirs in its western and northern regions. The gas reservoir development in the S6 well area (central region), which has higher hydrocarbon generation intensity, is markedly better than in the western region. Gas–water reservoirs are more common in the area of weak hydrocarbon generation in the west, and there are almost no pure gas reservoirs in the S43 well area, which has the weakest hydrocarbon generation intensity. Gas test results show that in the western area of the Sulige gas field, where the intensity of hydrocarbon generation decreases from 24 $\times$ 10^8 m^3/km^2 in the south to 14 $\times$ 10^8 m^3/km^2 in the north, the water production of the gas wells increases gradually and the gas production decreases. In the S43 well area, where the intensity of hydrocarbon generation is the weakest, water production is generally higher than that of surrounding wells.

5.4 Reservoir physical properties control on gas–water separation

Given the insufficient hydrocarbon generation intensity in the Sulige gas field, the high-permeability sand bodies were conducive to the accumulation of natural gas. However, due to the overall low hydrocarbon generation intensity, natural gas would have become dispersed and filled the thick homogeneous sand bodies at relatively low saturation levels. The gas enrichment processes of tight reservoirs and reservoir properties indicate that for gas accumulation in high-quality sand bodies, with a low shale content and good physical properties, the initial pressure of gas filling is low, the migration resistance is small, and the gas saturation becomes high (Fig. 11). Conversely, sand bodies with a high shale content and poor physical properties mostly develop low gas saturation after filling, and gas–water co-layers, gas–water layers, or dry layers are mainly developed. The development of gas–water layers and the scale of the effective reservoirs in the Sulige gas field are obviously related to differences in reservoir physical properties. With a sufficient gas supply, the sand bodies with better physical properties have higher gas saturation and productivity, whereas the sand bodies with poor physical properties have higher water saturation and lower gas productivity (Rashid et al., 2015; Nazemi et al., 2019). With weak hydrocarbon generation intensity, high-permeability reservoirs with a low displacement pressure become preferentially filled to form pure gas reservoirs. Gas and gas–water layers are typically developed adjacent

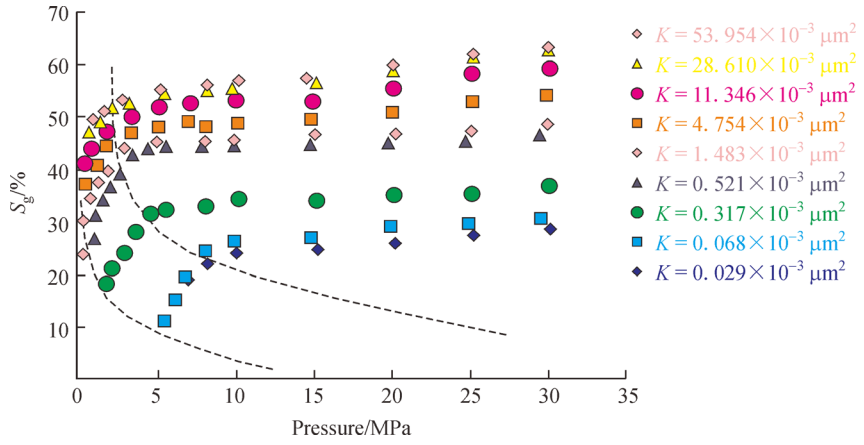

Fig. 10 Variations in gas saturation with gas source pressure for different types of reservoir filling experiments.

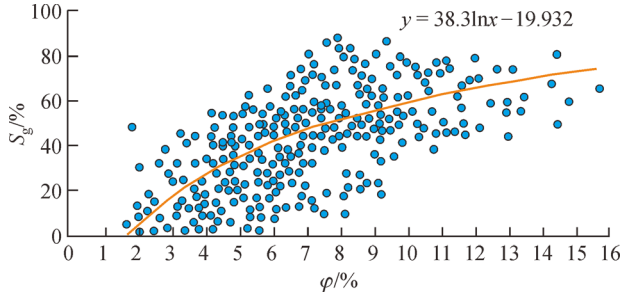

Fig. 11 Relationship between reservoir physical properties and gas-bearing properties.

to each other due to the large and abrupt changes in reservoir physical properties. Reservoirs formed of more pure lithologies that are porous and permeable form pure gas reservoirs, whereas the remaining sand bodies contain gas–water.

In the early stages of reservoir formation, the gas source conditions and reservoir quality have a large influence on the formation of gas reservoirs, and the role of tectonism is relatively minor (Bjørlykke, 2014; Landry et al., 2016; Ghanbarian et al., 2020). However, in the later stages of reservoir transformation, the role of tectonism becomes more important. The gas-rich "sweetspot" area with relatively complete gas–water differentiation and a large effective reservoir formed due to multi-stage tectonic modification. However, the "sweetspot" area is small in scale. The gas reservoirs located in structures with a low overall amplitude lack sufficient structural control, meaning that most wells produce both gas and water. This is because gas and water differentiation is controlled by the structural characteristics of the gas reservoir, and the H_8 Member reservoir has low permeability and is only weakly fractured. The structural range needed to form a pure gas cap is related to the reservoir conditions. The worse the pore throat condition and capillary force of a reservoir, the higher the gas–water transition zone, and a larger structural range is required to form a gas cap. In contrast, better reservoir physical properties require a smaller structural range to form a gas cap. As such, structural deformation is negatively correlated with reservoir physical properties. A capillary force test on type I, II, and III reservoirs allows the gas column height corresponding to the gas–water difference in various reservoirs to be calculated from the relationship between the J function (Eq. (4)) and water saturation (Eq. (5)). The results show that when the porosity is > 10%, the structural range required for complete gas–water differentiation is > 95 m. When the porosity is between 7.5% and 10%, the structural range required for complete gas–water differentiation is > 270 m. When the porosity is between 5% and 7.5%, the gas reservoir needs a structural range of ~385 m for complete gas–water differentiation (Fig. 12). In the Sulige gas field, the structural range is < 200 m, which is why gas–water is generally produced.

$$\mathrm{J} = \frac{P_c}{\sigma \cos\theta}\sqrt{\frac{K}{\phi}}, \tag{4}$$

$$S_w = ae^{bJ}, \tag{5}$$

where P_c is capillary pressure, Pa; σ is interfacial tension, mN/m; θ is wetting angle, ° ; S_w is water saturation, %; a, b are constants; K is permeability, × 10^{-3} μm²; φ is porosity, %.

6 Conclusions

1) The effective reservoir size of tight gas is relatively small, and the effective single sand body thickness, length, and width are 1–5, 200–500, and 400–700 m, respectively. Compared with conventional gas reservoirs, tight gas effective reservoirs are small in scale and have low gas saturation.

2) Due to sedimentary and diagenetic controls, the

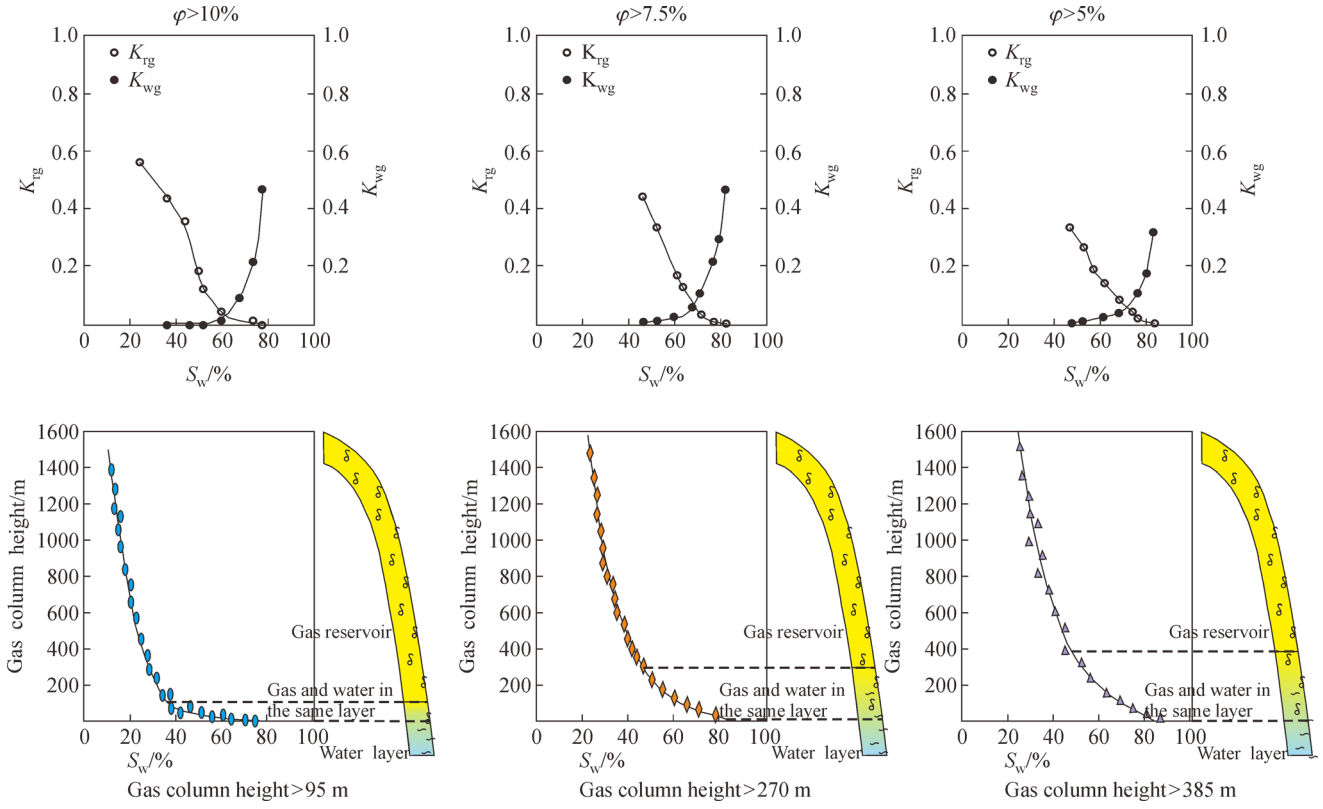

Fig. 12 Gas–water interface heights in different types of effective reservoirs.

effective reservoirs are highly dispersed and comprise high-permeability units within a generally low-permeability lithology. Sedimentary processes are the primary cause of the small scale of the effective reservoirs.

3) The effective reservoirs often exhibit macroscopic variations in gas–water distribution and gas production characteristics. Due to migration and accumulation, areas with high hydrocarbon generation intensity are mostly gas-enriched, and areas with low hydrocarbon generation intensity are mostly gas–water reservoirs.

4) Under weak hydrocarbon generation intensity conditions, high-permeability reservoirs with a low displacement pressure become preferentially filled to form pure gas reservoirs. Gas and gas–water layers typically develop adjacent to each other, due to the large and abrupt changes in reservoir physical properties.

5) Degraded pore characteristics and a lower capillary force in the reservoir result in a higher gas–water transition zone, and thus a larger structural range is required to form a gas cap. The type I, II, and III reservoirs have different gas–water separation heights. The structural ranges required for complete gas–water differentiation are >95, >270, and 385 m.

Acknowledgements This study was financially supported by the PetroChina Innovation Foundation (No. 2019D-5007-0210), National Natural Science Foundation of China (Grant Nos. 51904050、41902153), the Chongqing Natural Science Foundation Project (Nos. cstc2019jcyj-msxmX0725、0457), Open Fund of Engineering Research Center of Development and Management for Low to Ultra-Low Permeability Oil & Gas Reservoirs in West China, Ministry of Education (KFJJ-XB-2020-4) and the Science and Technology Research Program of Chongqing Municipal Education Commission (No. KJQN201901531).

References

Abdulrauf R A, Lamidi B, Syed R H, Abdullah A, Rahul S B (2019). Insight into the pore characteristics of a Saudi Arabian tight gas sand reservoir. Energies, 12(22): 1–27

Abuamarah B A, Nabawy B S, Shehata A M, Kassem O M K, Ghrefat H (2019). Integrated geological and petrophysical characterization of oligocene deep marine unconventional poor to tight sandstone gas reservoir. Mar Pet Geol, 109: 868–885

Amiri M, Yunan M H, Zahedi G, Jaafar M Z, Oyinloye E O (2012). Introducing new method to improve log derived saturation estimation in tight shaly sandstones—a case study from Mesaverde tight gas reservoir. J Petrol Sci Eng, 92–93: 132–142

Behmanesh H, Hamdi H, Clarkson C R (2015). Production data analysis of tight gas condensate reservoirs. J Nat Gas Sci Eng, 22: 22–34

Bersezio R, Giudici M, Mele M (2007). Combining sedimentological and geophysical data for high-resolution 3-D mapping of fluvial architectural elements in the Quaternary Po plain (Italy). Sediment Geol, 202(1–2): 230–248

Best J, Woodward J, Ashworth P, Smith G S, Simpson C (2006). Bar-top hollow: a new element in the architecture of sandy braided rivers.

Sediment Geol, 190(1-4): 241–255

Bjørlykke K (2014). Relationships between depositional environments, burial history and rock properties—some principal aspects of diagenetic process in sedimentary basins. Sediment Geol, 301: 1–14

Bridge J S (1993). The interaction between channel geometry, water flow, sediment transport and deposition in braided rivers. Geological Society, London, Special Publications, 75(1):1–71

Bridge J S, Tye R S (2000). Interpreting the dimensions of ancient fluvial channel bars, channels, and channel belts from wireline-logs and cores. AAPG Bull, 84: 1205–1228

Chen P, Tan X, Yang H, Tang M, Jiang Y, Jin X, Yu Y (2015). Characteristics and genesis of the Feixianguan Formation oolitic shoal reservoir, Puguang gas field, Sichuan Basin, China. Front Earth Sci, 9(1): 26–36

Daniel A, Viktor R (2015). Investigation on fluid transport properties in the North-German Rotliegend tight gas sandstones and applications. Environ Earth Sci, 15: 4322–4331

Davy C A, Skoczylas F, Barnichon J D, Lebon P (2007). Permeability of macro-cracked argillite under confinement: gas and water testing. Phys Chem Earth, 32(8–14): 667–680

Economides M J, Wood D A (2009). The state of natural gas. J Nat Gas Sci Eng, 1(1-2): 1–13

Fan X, Gong M, Zhang Q, Wang J, Bai L, Chen Y (2014). Prediction of the horizontal stress of the tight sandstone formation in eastern Sulige of China. J Petrol Sci Eng, 113: 72–80

Fu X, Agostini F, Skoczylas F, Jeannin L (2015). Experimental study of the stress dependence of the absolute and relative permeabilities of some tight gas sandstones. Int J Rock Mech Min Sci, 77: 36–43

Ghanbarian B, Liang F, Liu H (2020). Modeling gas relative permeability in shales and tight porous rocks. Fuel, 272: 1–11

Guo C, Xu J, Wei M, Jiang R (2015). Experimental study and numerical simulation of hydraulic fracturing tight sandstone reservoirs. Fuel, 159: 334–344

Guo Z, Jia A, Ji G (2017). Reserve classification and well pattern infilling method of tight sandstone gasfield: a case study of Sulige. Acta Petrol Sin, 38: 1299–1309

He D, Jia A, Ji G, Wei Y, Tang H (2013). Well type and pattern optimization technology for large scale tight sand gas, Sulige gas field. Pet Explor Dev, 40(1): 84–94

Hooke J (2003). Coarse sediment connectivity in river channel systems: a conceptual framework and methodology. Geomorphology, 56(1–2): 79–94

Hu W, Wei Y, Bao J (2018). Development of the theory and technology for low permeability reservoirs in China. Pet Explor Dev, 45(4): 685–695

Ji G, Jia A, Meng D, Guo Z, Wang G, Cheng L, Zhao X (2019). Technical strategies for effective development and gas recovery enhancement of a large tight gas field: a case study of Sulige gas field, Ordos Basin, NW China. Pet Explor Dev, 46(3): 629–639

Jia A, Wang G, Meng D, Guo Z, Ji G, Cheng L (2018). Well pattern infilling strategy to enhance oil recovery of giant low-permeability tight gasfield: a case study of Sulige gasfield, Ordos Basin. Acta Petrol Sin, 39: 802–813

Jiang S, Chen P, Yan M, Liu B, Liu H, Wang H (2020). Model of effective width and fracture conductivity for hydraulic fractures in tight reservoirs. Arab J Sci Eng, 20(4): 614–628

John W R, Peter J M (1997). Sandstone-body and shale-body dimensions in a braided fluvial system: Salt Wash Sandstone Member (Morrison Formation), Garfield County, Utah. AAPG Bull, 81: 1267–1291

Ju W, Shen J, Qin Y, Meng S, Li C, Li G, Yang G (2018). *In-situ* stress distribution and coalbed methane reservoir permeability in the Linxing area, eastern Ordos Basin, China. Front Earth Sci, 12(3): 545–554

Labourdette R (2011). Stratigraphy and static connectivity of braided fluvial deposits of the lower Escanilla Formation, south central Pyrenees, Spain. AAPG Bull, 95(4): 585–617

Landry C J, Prodanović M, Eichhubl P (2016). Direct simulation of supercritical gas flow in complex nanoporous media and prediction of apparent permeability. Int J Coal Geol, 159: 120–134 doi:10.1016/j.coal.2016.03.015

Li H, Li Y, Feng Y, Zhong J, Luo H (2020a). An interpretation method for a gas production profile based on the temperature and pressure behavior of low-permeability gas reservoirs. Arab J Sci Eng, 20(4): 545–565

Li Y, Yang J, Pan Z, Meng S, Wang K, Niu X (2019a). Unconventional natural gas accumulations in stacked deposits: a discussion of Upper Paleozoic coal-bearing strata in the east margin of the Ordos Basin, China. Acta Geol Sin, 93(1): 111–129

Li Y, Gao X, Meng S, Wu P, Niu X, Qiao P, Elsworth D (2019b). Diagenetic sequences of continuously deposited tight sandstones in various environments: a case study from Upper Paleozoic sandstones in the Linxing area, eastern Ordos basin, China. AAPG Bull, 103(11): 2757–2783

Li Y, Xu W, Wu P, Meng S (2020b). Dissolution versus cementation and its role in determining tight sandstone quality: a case study from the Upper Paleozoic in northeastern Ordos Basin, China. J Nat Gas Sci Eng, 78: 103324

Liu M, Liu Z, Wang B, Sun X, Guo J (2015a). A new method for recovering paleoporosity of sandstone: case study of middle Es_3 member of Paleogene formation in Niuzhuang Sag, Dongying Depression, Bohai Bay Basin in China. Front Earth Sci, 9(3): 521–530

Liu X, Kang Y, Luo P, You L, Tang Y, Kong L (2015b). Wettability modification by fluoride and its application in aqueous phase trapping damage removal in tight sandstone reservoirs. J Petrol Sci Eng, 133: 201–207

Liu Z, Cui M, Fan A (2014). Calculation method discussion of tight sandstone gas reserves: a case of volumetric method in SX block. Nat Gas Geosci, 25: 1983–1993

Lunt I A, Smith G H S, Best J L, Ashworth P J, Lane S N, Simpson C J (2013). Deposits of the sandy braided South Saskatchewan River: Implications for the use of modern analogs in reconstructing channel dimensions in reservoir characterization. AAPG Bull, 97(4): 553–576

Luo C, Jia A, Guo J, He D, Wei Y, Luo S (2016a). Analysis on effective reservoirs and length optimization of horizontal wells in the Sulige Gasfield. Nat Gas Ind, 3(3): 245–252

Luo C, Jia A, He D (2016b). Comparison study on the distribution of gas and water in Xu-4 and Xu-6 Formations tight gas sandstone reservoir of Guang'an Gasfield, Sichuan Basin. Nat. Gas Geosci., 27: 359–370

Martin R G (2006). Width and thickness of fluvial channel bodies and

valley fills in the geological record: a literature compilation and classification. J Sediment Res, 76(5): 731–770

Miall A D (2006). Reconstructing the architecture and sequence stratigraphy of the preserved fluvial record as a tool for reservoir development: A reality check. AAPG Bull, 90(7): 989–1002

Miller M, Shanley K (2010). Petrophysics in tight gas reservoirs-key challenges still remain. Lead. Edge, 29(12): 1464–1469

Morad S, Al-Ramadan K, Ketzer J M, De Ros L (2010). The impact of diagenesis on the heterogeneity of sandstone reservoirs: a review of the role of depositional facies and sequence stratigraphy. AAPG Bull, 94(8): 1267–1309

Morteza A, Gholamreza Z, Mat H Y (2015). Reducing predictive uncertainty in log-derived water saturation models in a giant tight shaly sandstones-A case study from Mesaverde tight gas reservoir. J Nat Gas Sci Eng, 23: 380–386

Nazari M H, Tavakoli V, Rahimpour-Bonab H, Sharifi-Yazdi M (2019). Investigation of factors influencing geological heterogeneity in tight gas carbonates, Permian reservoir of the Persian Gulf. J Petrol Sci Eng, 183: 1–18

Nazemi M, Tavakoli V, Sharifi-Yazdi M, Rahimpour-Bonab H, Hosseini M (2019). The impact of micro-to macro-scale geological attributes on Archie's exponents, an example from Permian–Triassic carbonate reservoirs of the central Persian Gulf. Mar Pet Geol, 102: 775–785

Nelson P H (2009). Pore-throat sizes in sandstones, tight sandstones and shales. AAPG Bull, 93(3): 329–340

Ostensen R W (1983). Microcrack permeability in tight gas sandstone. SPE J, 23(6): 919–927

Rashid F, Glover P W J, Lorinczi P, Collier R, Lawrence J A (2015). Porosity and permeability of tight carbonate reservoir rocks in the north of Iraq. J Petrol Sci Eng, 133: 147–161

Santamarina J C, Park J, Terzariol M, Cardona A, Castro G M, Cha W, Garcia A, Hakiki F, Lyu C, Salva M, Shen Y, Sun Z, Chong S H (2019). Soil Properties: Physics Inspired, Data Driven. In Lu N, Mitchell J, eds. Geotechnical Fundamentals for Addressing New World Challenges. Cham: Springer: 67–91

Shanley K W, Cluff R M, Robinson J W (2004). Factors controlling prolific gas production from low-permeability sandstone reservoirs: implications for resource assessment, prospect development, and risk analysis. AAPG Bull, 88(8): 1083–1121

Skelly L R, Bristow S C, Ethridge G F (2003). Architecture of channel-belt deposits in an aggrading shallow sandbed braided river: the lower Niobrara River, northeast Nebraska. Sediment Geol, 158(3–4): 249–270

Smith S H G, Ashworth J P, Best L J, Woodward J, Simpson J C (2006). The sedimentology and alluvial architecture of the sandy braided South Saskatchewan River, Canada. Sedimentology, 53(2): 413–434

Tye R S (2004). Geomorphology: an approach to determining subsurface reservoir dimensions. AAPG Bull, 88(8): 1123–1147

Wang G, Jia A, Yan H (2017). Characteristics and recoverability evaluation on the potential reservoir in Sulige tight sandstone gas field. Oil Gas Geol., 38: 896–904

Wang H, Jiang S, Huang C (2018). Differences in sedimentary filling and its controlling factors in rift lacustrine basins, East China: a case study from Qikou and Nanpu sags. Front Earth Sci, 5(1): 82–96

Wang J, Jiang S, Jun X (2020). Lithofacies stochastic modelling of a braided river reservoir: a case study of the Linpan Oilfield, Bohaiwan Basin, China. Arab J Sci Eng, 20(4): 577–590

Xu X, Hu Y, Shao L (2017). Experimental simulation of gas accumulation mechanism in sandstone reservoir: a case study of Sulige gas field, Ordos Basin. J China U Min Technol, 46: 1323–1331

Yuan L, Sima L, Wu S (2014). Models for saturation of the tight gas sandstone reservoir. Petrol Sci Technol, 32(23): 2777–2785

Zafar A, Su Y, Li L, Fu J, Mehmood A, Ouyang W, Zhang M (2020). Tight gas production model considering TPG as a function of pore pressure, permeability and water saturation. Petrol Sci, 17(5): 1356–1369

Zhao F, Tang H M, Meng Y F, Li G, Xing X (2009). Damage evaluation for water-based underbalanced drilling in low-permeability and tight sandstone gas reservoirs. Pet Explor Dev, 36(1): 113–119

Zhao W, Bian C, Xu Z (2013). Similarities and differences between natural gas accumulations in Sulige gas field in Ordos basin and Xujiahe gas field in Central Sichuan Basin. Pet Explor Dev, 40(4): 429–437

Ziarani A S, Aguilera R (2012). Pore-throat radius and tortuosity estimation from formation resistivity data for tight-gas sandstone reservoirs. J Appl Geophys, 83: 65–73

Zou C, Yang Z, Zhang G (2019). Establishment and practice of unconventional oil and gas geology. Acta Geol Sin, 93: 12–23

Zou C, Zhu R, Liu K, Su L, Bai B, Zhang X, Yuan X, Wang J (2012). Tight gas sandstone reservoirs in China: characteristics and recognition criteria. J Petrol Sci Eng, 88–89: 82–91